3

ECM and EDM

A comparative study of the ANN and RSM models for predicting process parameters during WEDC of SiC_p/6061 Al MMC

Pragya Shandilya[1], P.K. Jain[1] and N.K. Jain[2]
[1] Department of Mechanical and Industrial Engineering, Indian Institute of Technology, Roorkee, 247667, India
[2] Department of Mechanical Engineering, Indian Institute of Technology, Indore, 452017, India

Abstract. Metal matrix composites (MMCs) have found many successful industrial applications in recent past as high-technology materials due to their properties. Wire electric discharge cutting (WEDC) process is considered to be one of the most suitable processes for machining MMCs. Lot of research work has been done on WEDC, but very few investigations have been done on WEDC of MMCs. This paper reports work on the analysis of material removal rate (MRR) and cutting width (kerf) during WEDC of 6061 Al MMC reinforced with silicon carbide particles (i.e. SiC_p/6061 Al). Four WEDC parameters namely servo voltage (*SV*), pulse-on time (T_{ON}), pulse-off time (T_{OFF}) and wire feed rate (*WF*) were chosen as machining process parameters. Artificial neural network (ANN) models and response surface methodology (RSM) models were developed to predict the MRR and kerf using Box-Behnken design (BBD) to generate the input/output database. It was observed that prediction of responses from both models closely agree with the experimental values. The ANN models and RSM models for WEDC of MMC were compared with each other on the basis of prediction accuracy which shows that ANN models are more accurate than RSM models for MRR and kerf because the values of percentage absolute errors are higher for RSM models than ANN models.

Keywords: Artifical neural network, Response surface methodology, Wire electric discharge cutting, Metal matrix composites, Material removal rate, kerf.

1. Introduction

Concerning industrial applications, MMCs now have a proven record of accomplishment as successful high-technology materials due to the properties such as high strength-to-weight ratio, high toughness, lower value of coefficient of thermal expansion, good wear resistance, and capability of operating at elevated temperatures [1]. MMCs are fabricated using several processes such as casting, forging and extrusion. However, cutting and finishing operations of MMCs are not well understood. The use of traditional machining processes to machine hard composite materials causes serious tool wear due to abrasive nature of reinforcing particles thus shortening tool life [2]. Although, nontraditional machining techniques such as water jet machining (WJM) and laser beam machining (LBM) can be used but the machining equipment is expensive, height of the workpiece is a constraint, and surface finish obtained is not good [3]. On the other hand, some techniques such as electric discharge machining (EDM) and wire electric discharge machining (WEDM) or wire electric discharge cutting (WEDC) are quite successful for machining of MMCs. EDM has limited applications as it can be used only for drilling purpose. WEDM which is a derived process of EDM seems to be a better choice as it conforms to easy control and can machine intricate and complex shapes. The setting for the various process parameters required in WEDC process play crucial role in achieving optimal performance. According to Patil and Brahmankar [4], during WEDC an accurate and efficient machining operation without compromising machining performance is achievable. Effective and economical WEDC of MMCs will open new areas of applications for MMCs. The most important performance measures in WEDC are MRR and kerf. In WEDC, the material removal is by melting and/or evaporation of electrically conductive phase of SiC_p/6061 Al MMC. kerf determines the dimensional accuracy of the finishing part. Extensive experimental work is therefore needed to analyze and optimize the process parameters to understand their effect on product quality. The current investigation aims at investigating the suitability of MRR and kerf predictive models based on RSM and ANN models during WEDC of SiC_p/6061 Al MMC.

2. Experimentation

The experiments were conducted on the ECOCUT WEDM machine from Electronica India Pvt Ltd. 6061 aluminum based MMC, made by stir casting technique having 10% SiC particles (by weight) as reinforcement were used as the workpieces. The workpieces were of rectangular shape having a thickness of 6 mm. The

S. Hinduja and L. Li (eds.), *Proceedings of the 37th International MATADOR Conference*,
DOI: 10.1007/978-1-4471-4480-9_3,

deionized water was used as dielectric. The dielectric temperature was kept at 20ºC. A diffused brass wire of 0.25 mm diameter was used as the cutting tool. The four input process parameters namely servo voltage *(SV)*, pulse-on time *(T_{ON})*, pulse-off time *(T_{OFF})* and wire feed rate *(WF)* were chosen as variables to study their effect on the quality of cut in SiC_p/6061 Al MMC during WEDC. The ranges of these parameters were selected based on literature survey, machining capability and preliminary experiments conducted by using one-variable-at-a-time approach [5]. Table 1 gives the levels of various parameters and their designation.

To calculate the MRR, the following equation [6] is considered:

$$MRR = \frac{Mf - Mi}{\rho t} \quad (1)$$

where, *Mi*, are masses (in gm) of the work material before and after machining respectively, ρ is the density of workpiece material and t is the time of machining in minutes. An electronic weighing machine with an accuracy of 0.001 mg is used to weight the material. The kerf was measured using the stereo microscope, and is expressed as sum of wire diameter and twice of wire-workpiece gap.

Table 1. Levels of process parameters

Process parameters	Levels		
	-1	**0**	**+1**
Voltage (V)	70	80	90
Pulse-on time (µs)	1	2	3
Pulse-off time (µs)	6	8	10
Wire feed (m/min)	5	7	9

The WEDC process was studied according to the Box-Behnken design (BBD). In this investigation, total 29 experiments were conducted. Levels and values of four process parameters for 29 experimental runs were given in Table 1.2. The 'Design Expert 6.0' software was used to establish mathematical models for optimization of the parameter settings to achieve the required MRR and kerf during WEDC of SiC_p/6061 Al MMC.

3. RSM based predictive models

Mathematical models based on RSM for correlating responses such as MRR and kerf with various settings of process parameters during WEDC of SiC_p/6061 Al MMC have been established, and are represented in the following regression equations

$$MRR = +2239.042 - 3.650SV - 12.115T_{OFF} - 9.427WF + 0.0134SV^2 + 0.248T_{OFF}^2 + 0.228WF + 0.0980VT_{OFF} + 0.077VWF \quad (2)$$

$$kerf = -6.016 + 0.097SV + 0.095T_{ON} + 0.272T_{OFF} + 0.325WF - 0.004SV^2 - 0.022T_{ON}^2 - 0.006T_{OFF}^2 - 0.008WF^2 + 0.009SVT_{ON} - 0.001SVT_{OFF} - 0.008SVWF - 0.007T_{ON}T_{OFF} - 0.004T_{ON}WF - 0.007T_{OFF}WF \quad (3)$$

Table 2 shows the RSM predicted values for MRR and kerf for the 29 experimental runs.

Table 2. BBD with four parameters and experimental MRR and kerf

Exp. No.	SV	T_{ON}	T_{OFF}	WF	MRR (mm^3/min)	Kerf (mm)
1	0	1	0	-1	4.200	0.381
2	-1	0	0	-1	9.965	0.266
3	0	0	1	1	4.931	0.328
4	-1	0	1	0	5.188	0.287
5	0	-1	-1	0	4.586	0.359
6	1	0	0	-1	3.679	0.415
7	1	0	-1	0	3.026	0.438
8	0	0	0	0	3.243	0.424
9	0	0	0	0	3.943	0.387
10	1	0	0	1	5.072	0.308
11	0	0	1	-1	3.897	0.407
12	0	0	0	0	3.939	0.394
13	0	-1	0	1	4.740	0.342
14	0	0	0	0	3.170	0.426
15	0	1	0	1	5.075	0.302
16	0	0	0	0	3.293	0.422
17	1	0	1	-1	4.702	0.352
18	0	1	-1	-1	4.974	0.322
19	0	0	-1	1	4.340	0.368
20	0	-1	0	-1	4.251	0.372
21	0	0	-1	-1	4.851	0.334
22	0	-1	1	0	3.901	0.401
23	1	1	0	0	2.590	0.446
24	-1	0	-1	0	11.354	0.261
25	-1	1	0	0	5.991	0.274
26	-1	0	0	1	5.126	0.294
27	-1	-1	0	0	5.325	0.282
28	1	-1	0	0	3.132	0.432
29	0	1	1	0	4.997	0.316

4. Development of ANN models for prediction of responses

An ANN is an information-processing system that has certain performance characteristics in common with biological neural networks. Generally, an ANN is made up of some neurons connected together via links. Among various neural network models, the feedforward neural network based on back-propagation is the best general-purpose model [7]. The network has four inputs of servo voltage (*SV*), pulse-on time (*T_{ON}*), pulse-off time (*T_{OFF}*), wire feed rate (*WF*) and two outputs of MRR and kerf. The training of the ANN for 29 input-output patterns has been carried out using the Neural Network Toolbox available in MATLAB software package. The network consists of one input layer, one hidden layer and one

output layer. In the proposed model, there were four input variables and two outputs. Hence the number of input neurons was taken as four and the number of output neurons was two. The selection of number of neurons in the hidden layer is usually model dependent. The numbers of hidden layers neurons are decided by trial and error method on the basis of the improvement in the error with increasing number of hidden nodes [8]. Hence, there were fifteen neurons in hidden layer. To train each network, an equal learning rate and momentum constant (α) of 0.05 and 0.9 respectively were used, the activation function of hidden and output neurons was selected as a hyperbolic tangent, and the error goal (mean square error, MSE) value was set at 0.0001, which means the training epochs are continued until the MSE fell below this value. To calculate connection weights, a set of desired network output values is needed. Desired output values referred as training dataset, obtained with the help of design of experiments (DOE). MRR and kerf values corresponding to training data were obtained from experimental runs generated by BBD based on RSM. The dataset generated by BBD shown in Table 2. Table 3 shows ANN predicted values for MRR and kerf for the 29 training set.

5. Comparison of the RSM and ANN models

An attempt was made to compare the RSM and ANN predicted models on the basis of their prediction accuracy. The RSM and ANN models were tested with 29 data sets of BBD of experiments. For each input combination, the predicted values of responses were compared with the respective experimental values and the absolute percentage error is computed as follows:

$$\text{percentage absolute error} = \frac{Yj,expt - Yj,pred}{Yj,expt} * 100 \qquad (4)$$

Where *Yj,expt* is the experimental value and *Yj,pred* is the predictive value of the response for the jth trail by the RSM and ANN models. The absolute percentage error were found for ANN and RSM models and maximum values of error for MRR and kerf were tabulated in Table 4. From this table it can be concluded that ANN predictions are more accurate than RSM predictions because the values of maximum percentage absolute error are less for ANN models than RSM models for each response parameter. Figure 1 illustrate the comparison of error profile for responses, for the 29 data set of the training patterns. From this figure it has been observed that ANN predictions are better than the RSM predictions.

In order to test the interpolation of the prediction from the developed models, experimetnal MRR and kerf values were compared with the predicted values of the ANN and RSM models. This comparison is shown in Fig. 2. It is observed from this figure that the prediction of responses from both models closely agree with that of experimental values.

An attempt was also made to compare the RSM and ANN models on the basis of correlation coefficient. Table 4 lists the values of correlation coefficients for ANN and RSM models of each response parameter. The correlation coefficient between the experimental values and predicted values is a measure of how well the variation in the predicted values is explained by the experimental values. The value of correlation coefficient equal to 1 indicates the perfect correlation between the experimental values and the predicted values. In most cases, the value of correlation coefficient is more closer to unity for ANN models for response parameters. Which clearly indicates that prediction accuracy is higher for ANN model compared to RSM model.

Table 3. List of ANN predictions and RSM predictions for MRR and kerf

Exp no.	MRR (mm^3/min)		kerf (mm)	
	ANN prediction	RSM prediction	ANN prediction	RSM prediction
1	4.2685	4.358	0.3753	0.371
2	9.9197	8.9887	0.2697	0.2549
3	5.0303	4.763	0.3285	0.2989
4	5.185	4.9591	0.2959	0.3049
5	4.6744	5.0357	0.3628	0.353
6	3.6631	2.4133	0.4283	0.4481
7	2.957	2.6882	0.4379	0.4196
8	3.5045	3.4473	0.4077	0.4077
9	3.5045	3.4473	0.4077	0.4077
10	4.9932	5.5341	0.3162	0.3322
11	3.8746	4.7583	0.4134	0.4038
12	3.5045	3.4473	0.4077	0.4077
13	4.6485	4.3631	0.3605	0.3516
14	3.5045	3.4473	0.4077	0.4077
15	4.9805	4.3631	0.2922	0.3124
16	3.5045	3.4473	0.4077	0.4077
17	4.6683	4.7738	0.3419	0.4317
18	5.0936	5.9467	0.3254	0.3271
19	4.385	5.9515	0.3758	0.3586
20	4.2335	4.3583	0.3715	0.3755
21	4.8143	5.9467	0.3266	0.3362
22	4.0098	3.8472	0.3853	0.388
23	2.682	3.0603	0.445	0.3989
24	11.2925	10.0686	0.265	0.2522
25	5.9127	6.5197	0.2727	0.2614
26	5.217	5.8775	0.2907	0.2883
27	5.3344	6.5197	0.276	0.3022
28	3.1771	3.0603	0.4242	0.4018
29	4.9813	3.8472	0.32	0.335

Table 4. Percentage absolute error and correlation cofficients for between RSM and ANN model

Percentage absolute error	MRR		kerf	
	ANN	RSM	ANN	RSM
	11	35	6	15
Correlation coefficient	MRR		kerf	
	ANN	RSM	ANN	RSM
	0.989	0.869	0.939	0.984

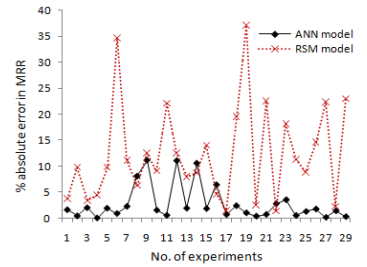

a

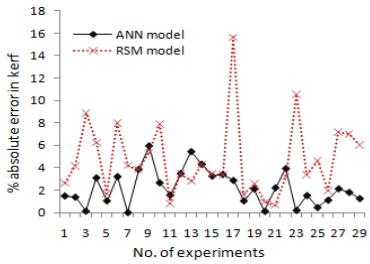

b

Fig. 1. Comparison of error profile for RSM and ANN model a) for MRR b) for kerf

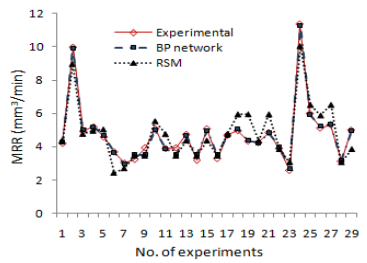

a

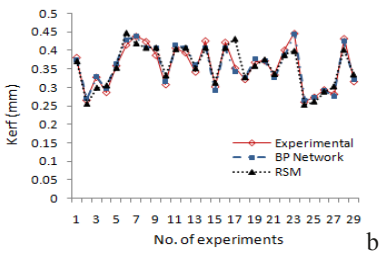

b

Fig. 2. Comparison of experimental measurements with predicted results from RSM and ANN model a) for MRR b) for kerf

6. Conclusions

Present study reports prediction of MRR and kerf through RSM and ANN techniques. RSM predicted values and ANN predicted values of MRR and kerf were compared with the experimental values to decide the nearness of prediction with the experimental values. Good agreement was obtained between the predicted values of both models and experimental measurements. Comparison of RSM models with ANN models on the basis of their prediction accuracy shows that ANN models are more accurate than RSM models for each response parameter because the values of percentage absolute error is higher for RSM models than ANN models. Comparison of RSM models with ANN models on the basis of correlation cofficients shows that in most cases the values of correlation coefficients are more closer to unity for ANN models. Which clearly indicates that ANN models are more accurate than RSM models because the value of correlation coefficients are almost equal to 1. This indicates a perfect correlation between the experimental values and the predicted values.

References

[1] Rosso M (2006) Ceramic and metal matrix composites: routes and properties. Journal of Materials Processing Technology 175: 364-375.

[2] Yan BH and Wang CC (1993) Machinability of SiC particle reinforced aluminum alloy composite material. Journal of Japan Institute Light Metals 43: 187-192.

[3] Lau WS and Lee WB (1991) Comparison between EDM wire cut and laser cutting of carbon fiber composite materials. Materials and Manufacturing Processes 6: 331-342.

[4] Patil NG and Brahmankar PK (2010) Some studies into wire electro-discharge machining of alumina particulate reinforced aluminum matrix composites. International Journal of Advanced Manufacturing Technology 48: 537-555.

[5] Shandilya P, Jain NK, Jain PK (2011) Experimental studies on WEDC of SiCp/6061 Al metal matrix composite, key Engineering Materials 450: 173-176.

[6] Neto JCS, Silva EM and Silva MB (2006) Intervening variables in electrochemical machining. Journal of Materials Processing Technology 179: 92-96.

[7] Hassoun MH (1995) Fundamentals of artificial neural networks. MIT Press.

[8] Benardos PG and Vosniakos GC (2003) Predicting surface roughness in machining: a review, International Journal of Machine Tools and Manufacture 43: 833-844.

Improved surface properties of EDM components after irradiation by pulsed electrons

J. Murray[1] and A.T Clare[1]
[1]Precision Manufacturing Centre, Department of M3, University of Nottingham, Nottingham, UK, NG7 2RD

Abstract. Electrical discharge machining (EDM) is a useful process for producing high aspect ratio features for components such as mold tools. The recast layer produced by rapid quenching however is often undesirable in engineering components due to its brittleness, the occurrence of cracking as well as high surface roughness, which contribute to reducing the part's overall fatigue and corrosion resistance. In the case of high aspect ratio geometries, recast layer removal via chemical etching then mechanical grinding is not always possible. In this study we investigate the use of the large-area electron beam irradiation technique to improve the properties of the EDM'd surface of a stainless steel so that a more desirable recast layer may be produced. As well as improvement in surface roughness, repair of EDM induced surface cracks was observed the and mechanism of this repair is discussed.

Keywords: EDM, recast layer, crack repair, polishing, electron beam melting

1. Introduction

EDM is a widely used process for the production of mould tools and engineering components involving high-aspect ratios and conformal geometries. During the process much of the material melted during discharge on-time is not removed but resolidified as a recast layer, with properties often undesirable in engineering applications. These include high roughness, brittleness as well as surface cracks. Reducing the extent of this layer is a continued goal of EDM research, given faster machining parameters usually yield a larger recast layer.

It has been shown that the presence of surface cracks induced by the EDM process can reduce the fatigue life of EDM'd components [1]. This is due to reducing the 2-stage fatigue failure process of crack formation then propagation into one stage of crack propagation. As well as the presence of cracks, surface features such as asperities and surface cavities which are stress concentrators are also known to have a strong influence on fatigue life [2, 3]. Uno et al. [4] showed that pulsed electron beam treatment of an EDM'd surface can reduce its roughness from 6μm Rz to under 1μm as well as improve its corrosion resistance. Okada et al. have more recently improved the corrosion resistance and blood repellency of surgical steel by this method [5]. The process has also been used to improve the wear resistance of aluminium based alloys [6]. TEM analysis of grain size by Zuo et al. [7] has shown grain size reduction to approximately 50nm can occur at the surface after irradiation, explaining the improved mechanical properties of such treated surfaces.

The potential for the elimination of surface cracks by this process as well as changes in phase and orientation of the EB treated surfaces of EDM'd components has not been assessed. This study therefore investigates the use of large-area electron beam irradaition for the potential of improving the fatigue life of EDM'd components via the suppression of surface cracks as well as the reduction of surface roughness of EDM'd surfaces.

2. Experimental

AISI 310 stainless steel was used as a workpiece material in this study. It is an austenitic, general purpose steel used widely in corrosive and high temperature applications. Surface roughness was measured by white-light interferometry (WLI) with a Fogale nanotech "Photomap 3D", and the Sa roughness parameter was used. XRD analysis was performed with a Bruker AXS D8 Advance" diffractometer using CuK (α) monochromatic radiation. Angles used were between 40º and 100º, with a step size of 0.04º. Electron microscopy was performed with a Hitachi S-2600 SEM.

2.1. EDM

A Sodick AP1L micro die-sink EDM machine was used to machine shallow slots in 310 stainless steel and induce a typical recast layer. Positive electrode polarity was used to best represent represent a typical EDM setup. Due to carbon adhesion onto tool electrodes in EDM using hydrocarbon dielectrics, minimal electrode wear is

associated with positive tool polarity [8]. A copper electrode was sunk 500µm into the workpiece as shown in Fig.

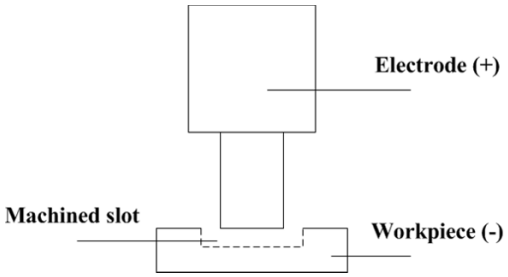

Fig. 1 Schematic of EDM operation

The chosen EDM parameters were based upon literature for EDM of features with dimension of the order of hundreds of microns [9], as well as previous experimental tests. The parameters used to produce the surface to be subject to electron irradiation are shown in Table 1.

Table 1 EDM Parameters

Electrode polarity	On-time (µs)	Off-time (µs)	Main current (A)	Gap voltage
+	30	3	4.5	90

2.2. Electron beam irradiation

Electron beam irradiation was performed using a Sodick PF32A "EBM". The process is carried in vacuum chamber into which Argon is supplied at a pressure of 0.05Pa. To produce the electron beam of 60mm diameter, a solenoid coil firstly produces a magnetic field, and at its maximum intensity a pulsed voltage is applied at the anode. Penning ionisation causes electrons to be generated which then move towards the anode. Argon atoms are then ionised by repeated collisions with electrons, generating plasma near the anode. When the intensity of this plasma is at a maximum, a pulsed voltage is applied to the cathode and electrons from the plasma are accelerated towards the workpiece. The bombardment of the electrons with the workpiece causes its surface to heat then rapidly quench.

Table 2 Electron beam parameters

Cathode voltage (kV)	No. of Shots	Anode voltage (kV)	Argon Pressure
25,35	1,5,10,20	5	4.5

The chosen EB parameters are shown in Table 2. Both the cathode voltage and the number of shots are vital parameters in this process, since the voltage determines the acceleration of electrons and therefore the energy density, while further shots repeat the process. Two cathode voltages were chosen based on previous experimental tests to represent medium and high power irradiation, with 1, 5, 10 and 20 shots for both settings.

3. Results and discussion

3.1. Surface roughness

The surface finish after irradiation was noticeably improved from the initial EDM surface, dominated by asperities and cracks. A before and after image with irradiation by 20 shots at 35kV is shown in Fig. 2.

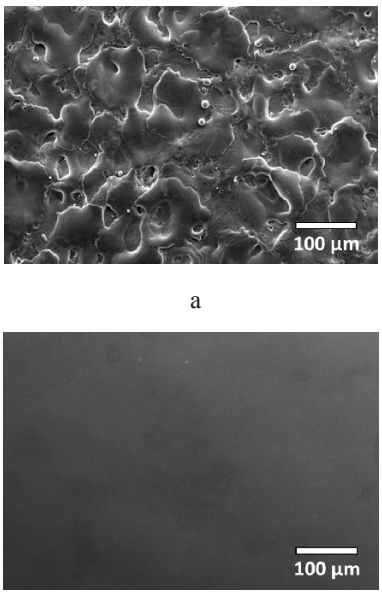

a

b

Fig. 2 EDM surface a) before and b) after irradiation

After measurement by WLI, the largest reduction in surface roughness occured after the highest number of shots of 20 at highest power of 35kV cathode voltage. A pre irradiation average roughness of 3.1µm Ra could be reduced to 0.9µm.

The trends in roughness according to increasing numbers of shots and the 2 cathode voltages are presented in Fig. 3. With both voltages there is a trend downwards for Sa roughness with increasing numbers of shots, although as expected the higher voltage parameter produces a more rapid improvement.

Crater formation commonly associated with the processing of materials by pulsed electron irradiation, and is well discussed in the literature was observed in our experiments. Under irradiation of 5 shots at 25kV as well as 20 shots at 35kV, craters were present. This phenomenon occurs due to melting which occurs below the surface, and the subsequent expansion and eruption from the surface. In steels this has been shown to occur at the location of carbides, which serve as nucleation sites

for sub-surface melting [10]. The frequency of crater formation as a result of this process is necessary to understand since they are known to accelerate pitting corrosion [11].

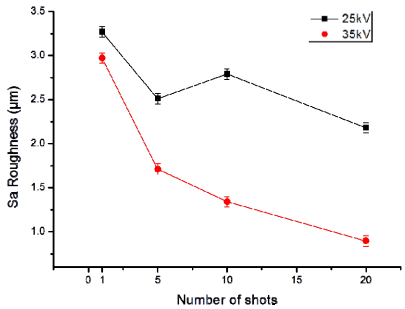

Fig. 3 Reduction in surface roughness with 25kV and 35kV cathode voltage irradiation

As well as the improvement in surface finish by the process, microscopy revealed a significant improvement in the proliferation of surface cracks. The next section quantifies and discusses this phenomenon.

3.2 Crack density

The change in surface crack density was quantified by SEM imaging of a statistically significant total area of 3.15mm^2, imaging then tracing the length of each individual crack in "ImageJ" image processing software. The total length of cracks for each sample was then divided by the total area to give the crack density. The results are shown in Fig. 4.

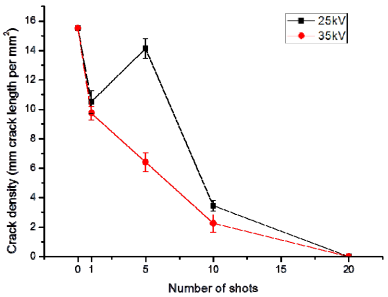

Fig. 4 Change in surface crack density after 25kV and 35kV cathode voltage irradiation

With 1 shot at both 25kV and 35kV cathode voltage, crack density was reduced. After 5 shots however, 25kV cathode voltage irradiation increased crack profileration to near control levels, which is likely due to the exposure of cracks previously repaired at the near surface by irradiation induced evaporation. Increasing numbers of shots at the higher cathode voltage of 35kV only reduced crack density, suggesting any evaporation taking place at the surface is not enough to compensate for the repairing effect of the irradation process. Further work is to be undertaken to assess the mass loss induced by the process. Surface images (15kV, 5 shots) were obtained tp elucidate the mechanism of repair. These can be seen in Fig. 5.

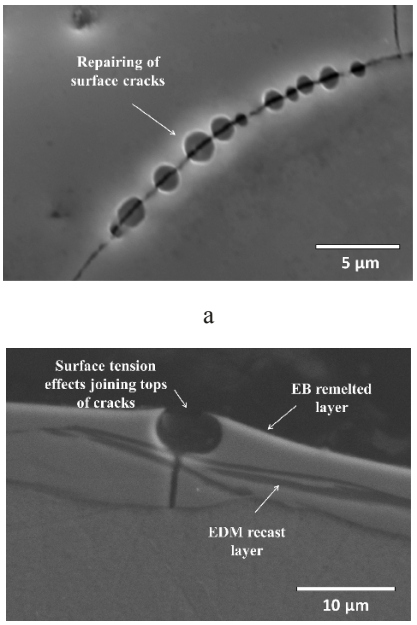

Fig. 5 Mechanism of repair of EDM surface cracks after irradiation

The rounded morphology of cracks at the surface subjected to low voltage irradiation suggests surface tension effects when both sides of the cracks are molten and are responsible for the merged features that are observed. This is supported by cross-sectional imaging, revealing the rounding of cracks into the recast layer with a narrow section joining at the very top surface. After 20 shots at 35kV voltage, there is no longer evidence of this effect, and no cracks are present in the newly re-melted layer as observed in the cross-section. The re-melted layer after 35kV and 20 shots, compared to the EDM'd material can be seen in Fig. 6.

It was observed that with these particular EDM settings, some of the initial recast layer remained unaffected at 35kV voltage and highest number of shots. This was beneath the uniform, newly re-melted layer produced by irradiation. In the unaffected EDM recast layer some cracking was observed, although penetration neither of the surface nor into the bulk occurred. It is thought that with improvements to the current irradiation process, specifically higher acceleration voltages, larger EDM layers can be re-melted, thus guaranteeing full depth of crack repair.

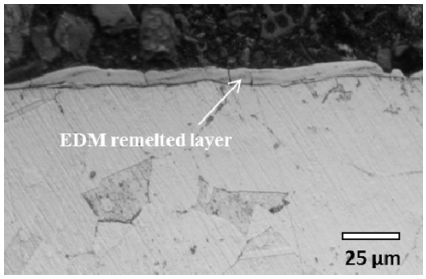

a

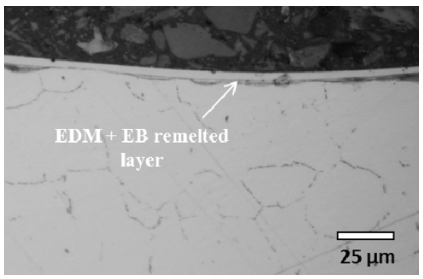

b

Fig. 6 Cross-section of a) EDM recast layer and b) uniform remelted layer after irradiation

3.3. XRD analysis

To assess any phase changes or changes in crystalline orientation at the surface, XRD analysis was performed on an EDM'd sample and a sample irradiated with 20 shots at 35kV. The XRD plot can be seen in Fig. 7.

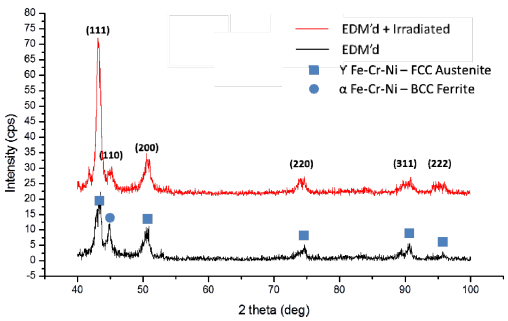

Fig. 7 XRD plot of EDM'd and irradiated surface. Significant crystalline texture is introduced after irradiation.

Significant crystalline texture is introduced by the irradiation process, with the (111) planes of the FCC phase orienting parallel to the surface. The ratio of intensities of the (111) to the (200) peak increases by a factor of 2.2. There is also a reduction in the strength of the BCC ferrite peak after irradiation. Crystalline texture at the surface has potential implications for the introduction of anisotropic layers for corrosion resistance, as has been shown by Shahryari et al. [12] whereby pitting corrosion resistance was improved in 316LVM stainless steel under (111) and (100) planar orientation.

4. Conclusions

Pulsed electron irradiation with a diameter of 60mm can be used to improve the surfaces of EDM'd stainless steel in approximately 15 minutes. Sa roughness of surfaces above 3µm can be reduced to below 1µm. Repair and elimination of surface cracks can occur in the newly re-melted surface. Crystalline texture can be introduced at the surface.

References

[1] Tai, T.Y. and S.J. Lu, Improving the fatigue life of electro-discharge-machined SDK11 tool steel via the suppression of surface cracks. International Journal of Fatigue, 2009. 31(3): p. 433-438.

[2] Andrews, S. and H. Sehitoglu, A computer model for fatigue crack growth from rough surfaces. International Journal of Fatigue, 2000. 22(7): p. 619-630.

[3] Rokhlin, S.I. and J.Y. Kim, In situ ultrasonic monitoring of surface fatigue crack initiation and growth from surface cavity. Int. Journal of Fatigue, 2003. 25(1): p. 41-49.

[4] Uno, Y., et al., High-efficiency finishing process for metal mold by large-area electron beam irradiation. Precision Engineering, 2005. 29(4): p. 449-455.

[5] Okada, A., et al., Surface finishing of stainless steels for orthopedic surgical tools by large-area electron beam irradiation. CIRP Annals - Manufacturing Technology, 2008. 57(1): p. 223-226.

[6] Walker, J., et al., Dry Sliding Friction and Wear Behaviour of an Electron Beam Melted Hypereutectic Al–Si Alloy. Tribology Letters, 2011: p. 1-10.

[7] Zou, J.X., et al., Microstructures and phase formations in the surface layer of an AISI D2 steel treated with pulsed electron beam. Journal of Alloys and Compounds, 2007. 434-435(0): p. 707-709.

[8] Kunieda, M. and T. Kobayashi, Clarifying mechanism of determining tool electrode wear ratio in EDM using spectroscopic measurement of vapor density. Journal of Mat. Processing Technology, 2004. 149(1-3): p. 284-288.

[9] Liu, H.-S., et al., A study on the characterization of high nickel alloy micro-holes using micro-EDM and their applications. Journal of Materials Processing Technology, 2005. 169(3): p. 418-426.

[10] Zou, J.X., et al., Cross-sectional analysis of the graded microstructure in an AISI D2-steel treated with low energy high-current pulsed electron beam. Applied Surface Science, 2009. 255(9): p. 4758-4764.

[11] Zhang, K., et al., Improved pitting corrosion resistance of AISI 316L stainless steel treated by high current pulsed electron beam. Surface and Coatings Technology, 2006. 201(3-4): p. 1393-1400.

[12] Shahryari, A., J.A. Szpunar, and S. Omanovic, The influence of crystallographic orientation distribution on 316LVM stainless steel pitting behavior. Corrosion Science, 2009. 51(3): p. 677-682.

Modeling and experimental study of electrical discharge diamond cut-off grinding (EDDCG) of cemented carbide

S. K. S. Yadav[1] and V. Yadava[2]
[1] Assistant Professor, MED, H.B.T.I Kanpur, India, sanjeevyadav10@rediffmail.com
[2] Professor, MED, MNNIT Allahabad, India, vinody@mnnit.ac.in

Abstract. This paper reports the development of neural network model and experimental study of electrical discharge diamond cut-off grinding (EDDCG) during machining of cemented carbide for average surface roughness (Ra). EDDCG is combination of diamond grinding and electrical discharge grinding. This process has been developed for machining of electrically conductive difficult to machine very hard materials such as cemented carbide, Ti-alloy, super alloys, metal matrix composites etc. ANN model was development for EDDCG process, to correlate the input process parameters such as current, pulse-on time, duty factor and wheel RPM with the performance measures namely, surface roughness. The experiments are carried out on a self developed electrical discharge diamond grinding setup in cut-off mode. The range of machining parameters was decided on the basis of pilot experiments. A total of 81 experiments were performed based on full factorial design of experiments. After experimentation the data set were divided into a training set and testing set for ANN modeling. Seventy present data of total available data set were used for training the network and remaining set were used for testing the network. The developed architecture can predict average surface roughness (Ra) with 0.0140 APE for training and 0.0042 APE for testing. Further, variation of surface roughness is plotted against different process parameters such as wheel RPM and pulse current.

Keywords: EDDCG, Ra, Cemented carbide, ANN Hybrid process.

1. Introduction

The Hybrid machining processes is defined as combination of two or more processes for shaping and finishing machine parts, it combining various physical and chemical processes acting on workpiece material into one machining process. These hybrid machining processes are developed to enhance advantages and to minimize potential disadvantages associated with an individual technique. Electrical discharge diamond grinding (EDDG) is a one of the hybrid machining process. It is a combination of diamond grinding and electrical discharge grinding (EDG). In this process metal bonded diamond grinding wheel is used. There are three basic configuration by which the combination of grinding and EDG can be classified. (1) Electro-Discharge Diamond Surface Grinding (EDDSG) (2) Electro-Discharge Diamond Face Grinding (EDDFG) (3) Electro-Discharge Diamond Cut-off Grinding (EDDCG). EDDSG is used to machine flat surfaces by using periphery of the metal bonded diamond grinding wheel. Since the work is normally held in a horizontal orientation, peripheral grinding is performed by rotating the grinding wheel about a horizontal axis. The relative motion of the workpiece is achieved by reciprocating the workpiece. EDDFG is used flat face of the metal bonded diamond grinding wheel. In this mode, the metal bonded diamond grinding wheel rotates about vertical spindle axis and fed in a direction perpendicular to the machine table. While machining, the rotating wheel is fed downwards under the control of servo system.

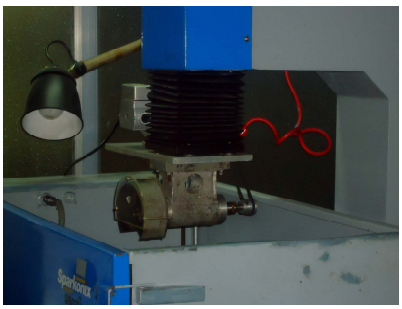

Fig.1. Electrical Discharge Diamond Grinding (EDDG) setup in cut-off grinding

EDDCG performed using periphery of the thin metal bonded diamond grinding wheel. While machining, the rotating wheel is fed downward using servo control, for material removal in cut-off configuration. Fig. 1 shows the self developed electrical discharge diamond grinding (EDDG) setup in cut-off mode. In this process metal bonded diamond grinding wheel was used. Sparking takes place between metallic bonding material and work piece. Heat generated during sparking and due to heat softens

the work material and hence machining by diamond abrasive particles becomes easier. Sparking in the inter electrode gap during EDDCG, results in continuous dressing of the grinding wheel and hence the wheel doesn't clog also. As a result cutting properties of the grinding wheel are stabilized. The projection of diamond grain on the bonding material of wheel is called protrusion height and gap between the work piece and bonding material is called gap width. For proper machining of work piece material, the protrusion height should be more then inter electrode gap [1].

2. Experimentation

Experiments were conducted on an EDM, attached with self developed grinding attachment of EDDCG. The set-up consists of a metal bonded diamond grinding wheel, D.C motor, shaft, V-belt and bearing, mounted on the ram of the machine to rotate the metal bonded grinding wheel about an axis. The rotating wheel is fed downwards under servo control, for material removal in the cut-off configuration. The thin metal bonded grinding wheel of 5.7mm and the work surface are physically separated by a gap, the magnitude of which depends on the local breakdown strength of the dielectric for a particular gap voltage setting [2]. Experiments were performed on cemented carbide workpiece. Four input parameters, such as current, pulse-on time, duty factor and wheel RPM and one output parameter, Ra chosen for modiling. According to the size of attachment, size of dielectric tank and requirement for machining of cemented carbide material, specification of diamond wheel shown in Table 1

Table 1. EDDCG Wheel specification

Wheel diameter	100 mm
Thickness of wheel	5.7 mm
Grit size	200/230
Concentration	75
Bonding	Bronze
Work material	Cement Carbide
Workpiece thickness	5.7 mm

It was decided to use full factorial design. The number of experiments to be performed using full factorial design can be given by formula [3].

$$N= F^k$$

where, N= is number of experiments, F= number of levels, k= number of factors

In the present work total of 81 (3^4) experiments have been performed and the value of Ra were taken. After experimentation the data set were divided into a training set and testing set for ANN modeling. The variation of Ra is plotted against different process parameters such as wheel RPM and pulse current.

3. ANN based modelling of EDDCG

The present work was aimed at establishment of correlation between input process parameters such as current, pulse-on time, duty factors and wheel speed with output parameter Ra. There are several algorithms in a neural network and the one that has been used in the present study is the back-propagation training algorithm. The back-propagation neural networks are usually referred to as feed forwarded, multilayered network with number of hidden layers. The error back–propagation process consists of two passes through the different layer of the network: a forward pass and a backward pass. In the forward pass, an activity pattern (input vector) is applied to the sensory nodes of the network, and its effect propagates through the network layer by layer. Finally, a set of output is produced as the actual response of the network. During the backward pass, all synaptic weights are adjusted in accordance with the error correction rule. Specifically the actual response of the network is subtracted from the desired (target) response to produce an error signal. The synaptic weights are adjusted so as to make the actual response of the network move closer to the desired network [4].

The steps of the ANN calculation during training using back propagation algorithm are as follows.

Step 1: The network synaptic weights are initialized to small random values.
Step 2: From the set of training input/output pairs, an input pattern is presented and the network response is calculated.
Step 3: The desired network response is compared with the actual output of the network, and all the local errors to be computed.
Step 4: The weights preceding each output node are updated according to the following update formula:

$$\Delta wij\ (t)= \eta\ \delta_i\ o_i + \alpha\ \Delta wij(t-1)$$

Where,η the learning rate, δ the local error gradient, α the momentum coefficient, o_i the output of the ith unit wij represents the weight connecting the ith neuron of the input vector and the jth neuron of the output vector. The local error gradient calculation depends on whether the unit into which the weights feed is in the output layer or the hidden layers. Local gradients in output layers are the product of the derivatives of the network's error function and the units' activation functions. Local gradients in hidden layers are the weighted sum of the unit's outgoing weights and the local gradients of the units to which these weights connect.

Step 5: The cycle (step 2 to step 4) is repeated until the calculated outputs have converged sufficiently close to

the desired outputs or an iteration limit has been reached.

The various signals are individually amplified, or weighted, and then summed together within the processing element. The resulting sum is applied to a specific transfer function, and the function value becomes the output of the processing element. Transfer function used in the back-propagation network is known as 'sigmoid function', which is shown below [5].

$$f(x) = \frac{1}{(1+e^{-x})}$$

where, X is the sum of the node input

The absolute prediction error (APE) is calculated using following equation [6].

$$APE(\%) = \left| \frac{Experimental\ result - ANN\ \Pr edicted\ result}{Experimental\ result} \right| \times 100$$

4. Training and testing of Neural network

Experiments were performed on cemented carbides workpiece. For the training and testing of the neural network, it is decided to use full factorial design, considering four input process parameters (current, pulse on-time, duty factor and wheel RPM) at three different levels, total of 81 (3^4) experiments have been performed and the value of Ra taken. After experimentation the data set were divided into a training set and testing set for ANN modeling. 70% data of total available data set were used for training the network and remaining used for testing the network. Before training and testing the total input and output data were normalized for increase accuracy and speed of the network. The datasets were normalized using the following equation.

$$X_n = \frac{X - X_{\min}}{X_{\max} - X_{\min}}$$

Where, X_n is the normalized value of variable X, X_{min} and X_{max} minimum and maximum value of X in total data sets.

First, neural network architecture has been decided, as there are four inputs and one outputs in the present problem, the number of neurons in the input and output layer has to set to four and one, respectively. As the number of hidden layer in the network increase, the complexity increases. Further single hidden layer gave comparatively better result with an optimum training time [5]. Hence, in the present case only one hidden layer has been considered.

In present problem the number of neurons in the hidden layer is changed and the total average prediction error for training and validation was calculated for each case.

Figure 2 shows the variation of APE with number of neurons in hidden layer in which the number of hidden neurons was varied from 3 to 19. The number of neurons in hidden layer is 18, for which the average prediction error is minimum.

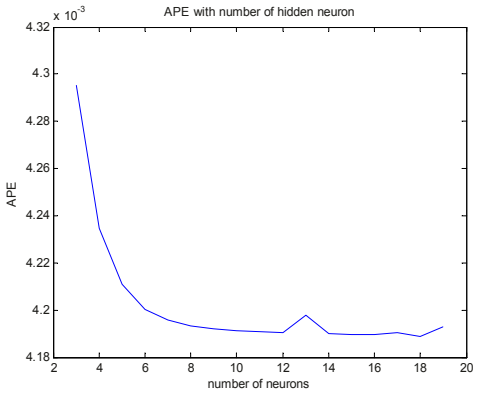

Fig. 2. Plot for determining the number of neurons in hidden layer

5. Results and discussions

The data were normalized to lie between 0 and 1.The model developed is a back-propagation network having 18 neurons in the hidden layer. Figure 3 shows the ANN architecture proposed for the present problem. It considers four inputs current, pulse on-time, duty factor, wheel RPM and one outputs Ra. So, 4-18-1 (4 input neurons, 18 hidden neurons and 1 output neurons) is the most suitable network selected for the present task with the help of self developed ANN based MATLAB code.

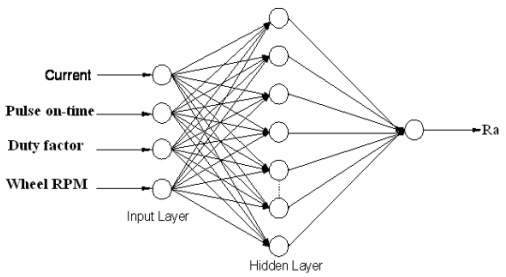

Fig. 3. The 4-18-1 ANN model for the Ra

The developed model was used to predict the output. During the training of network the learning rate taken as 0.01 to successfully train the network with maximum number of epochs 2000. The developed architectures 4-18-1 can predict Ra with 0.0140 APE for training and 0.0042 APE testing respectively shown in Fig. 4.

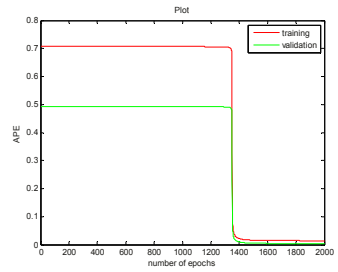

Fig. 4. The variation of APE with number of epochs

Figure 5 shows the variation of Ra with wheel RPM for different value of gap current. Here, Pulse on-time of 50 µs and duty factor of 0.5 was taken. It is observed that Ra decreases with increase in wheel RPM for all current values. This is due to increase in wheel RPM effective flushing of inter-electrode gap occurs and therefore, the adherence of resolidified eroded particles on the work surface is reduced and the resulting surface presents a better finish. It is also observed that for a particular wheel RPM, with increase in gap current, the R_a value is increases.

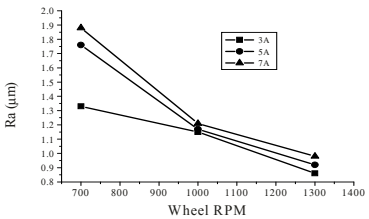

Fig. 5. Effect of wheel RPM on Ra for different currents during EDDCG

Figure 6 shows the variation of Ra with gap current for different values of wheel RPM. Here it is observed that the Ra increases with an increase in gap current for all value of wheel RPM. This is due to the simultaneous occurrence of flushing and efficient sparking material removal rate will increase as the energy input increases, resulting in bigger craters on the work surface and poor surface finish. At higher current increases in maximum protrusion height of grains also leads to deterioration of surface finish [7]. The SEM micrograph of machined surface at 1000 RPM and 5A are shown in Fig.7.

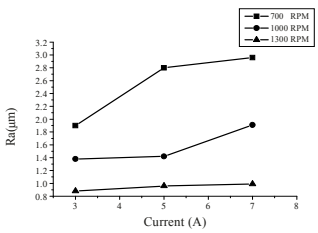

Fig.6. Effect of current on Ra for different RPM during EDDCG

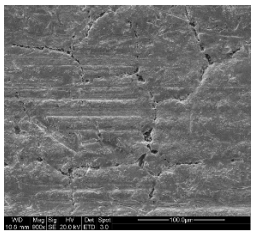

Fig. 7. Micrograph of machined surface observed under SEM

6. Conclusions

From the above results and discussion it can be concluded that: The developed architectures 4-18-1 can predict Ra with 0.0140 APE for training and 0.0042 APE testing respectively. Thus, it is apparent that the ANN model can be reliably used for prediction of output responses Ra in close conformity to the actual experimental data. An improvement in surface quality was found by 70% when wheel RPM is increase by 700 to 1300 RPM. For RPM range 700-1300 RPM if current is increased two times (from 3 to 7A).The Ra increase almost by a factor of 1.5 here the quality of surface detoriates for higher current. The experiments shows that better Ra achieve with lower range of pulse current with higher value of wheel RPM.

References

[1] Choudhary SK, Jain VK, Gupta M, (1999) Electrical discharge diamond grinding of high -speed steel : Mach. Sci. Tech. 3: 91-105

[2] Koshy P, Jain VK, Lal GK, (1997) Grinding of cemented carbide with electrical spark assistance. J. Mater. Process Technol. 72: 61-68

[3] Jain VK, Mote RG, (2005) On the temperature and specific energy during electro- discharge diamond grinding (EDDG): International Journal of Advanced Manufacturing Technology. 26: 56-67

[4] Jain RK, Jain VK, (2000) Optimum selection of machining condition in abrasive flow machining using neural network: J. Mater. Process Technol..108: 62-67

[5] Karunakar DB, Datta GL, (2008) Prevention of defects in castings using back propagation neural networks:.Int J Adv Manuf Technol. 39:1111-1124

[6] Dhara SK, Kuar AS, Mitra S, (2008) An artificial neural network approach on parametric optimization of laser micro-machining of die-steel: J.Adv. Manuf. Technol. 39:39-46

[7] Kumar S, Choudhury SK, (2007) Prediction of wear and surface roughness in electro-discharge diamond grinding: J. Mater. Process. Technol..191:206-20.

Experimental investigation on material removal rate in wire electrical discharge turning process for Al/SiC$_p$ metal matrix composite

M. Rajkumar[1], M. Kanthababu[2,*] and S. Gowri[3]
[1]PG Student, [2] Assistant Professor, [3] Professor
Department of Manufacturing Engineering, College of Engineering Guindy, Anna University, Chennai – 600 025,India.
*Corresponding author email: kb@annauniv.edu

Abstract. An attempt is made for the first time to machine metal matrix composite (MMC) consisting of aluminium alloy 360 (A360) reinforced with silicon carbide (SiC) particulate with 15 % volume fraction using wire electrical discharge turning (WEDT) process. WEDT is carried out by incorporating a rotary spindle attachment in the existing wire electrical discharge machine (WEDM). The experiments are carried out by Response Surface Methodology (RSM) using Box-Behnken method. The input machining parameters varied at three levels are pulse-on time (T_{ON}), gap voltage (V) and spindle speed (SS). The significant WEDT machining parameters and their levels are obtained for higher material removal rate (MRR) by using ANOVA and response surfaces. From this study, it is observed that high T_{ON}, medium V and low SS are resulted in higher MRR. Regression equation is established for the MRR for predication. The results obtained from this study will be useful to engineers in selecting the appropriate input WEDT parameters and their levels for cylindrical turning of MMC involving Al/SiC$_p$.

Keywords: Wire electrical discharge turning; Metal matrix composite; Response surface methodology; Material removal rate; ANOVA.

1. Introduction

Manufacturing industries today realise the need for generating different cylindrical forms in hard and difficult to machine materials especially composites. Hence, current researchers have made attempts to generate precise cylindrical forms using WEDT process in the conventional as well as hard to machine materials [1-9]. WEDT is type of hybrid machining processes generally carried out in WEDM by incorporating a rotary spindle attachment. WEDT process is found to have advantages over conventional turning process such as good repeatability, less deflection of workpiece due to non-contact process, elimination of stresses during machining, etc. In WEDT, the electrically charged wire is controlled by the x-y table of the WEDM and the rotational movement of the workpiece is controlled by the attached rotary motor which results in the removal of work material and generates desired cylindrical forms. Fine surface finish, less roundness error and enhanced material removal are possible by using significant WEDT process parameters.

Literature review indicates that researchers have studied the performance of WEDT process considering T_{ON}, pulse-off time (T_{OFF}), V and SS on MRR, surface roughness (R_a) and roundness error for different materials. It is observed that the selection of appropriate WEDT parameters for each material is a difficult task and it is material specific. It is also observed that there has been no attempt made to identify significant input WEDT process parameters for MMCs. MMCs have gained importance in various fields like aerospace, automobiles, defense, etc due to their superior properties [10]. The most commonly used MMC in different applications is found to be the combination of aluminium alloy reinforced with SiC (Al/SiC). The Al/SiC MMC in various cylindrical forms are expected to replace some of the existing materials in different applications. Therefore, in this work, an attempt has been made to indentify siginificant WEDT process parameters for generating cylindrical form in Al/SiC MMC.

2. Experimental details

Electronica make WEDM is used in this work, in which the WEDT setup is installed (Fig. 1). The WEDT set-up consists of various components such as self centering chuck, spindle shaft, deep groove single row ball bearings, spindle housing, DC motor (12V, 6W), timing belt, flanged gears and lock nut. The straight turning configuration is used in this work. The gap between the wire and workpiece is constantly maintained in the ranges between 0.075 mm to 0.1 mm by a CNC positioning system. The brass wire of 0.25 mm diameter is used as the electrode material. The depth of cut and the length of

the cut are maintained as 0.2 mm and 6 mm respectively. T_{OFF} and wire tension of 6 µs and 1.2 kgf respectively were kept statistically constant. Deionized water is used as dielectric fluid. The workpiece material used in this work is MMC consisting of A360 reinforced with 15% volume fraction of SiC particles (Al/SiC_p), which is prepared by stir casting process. The particle size of the reinforcement material is around 30 µm. Experiments are carried out by RSM [11] using Box-Behnken method in order to establish relationship between the WEDT process parameters and MRR (response). The important WEDT parameters such as T_{ON}, V and SS are varied at three levels (Table 1). The allocation of WEDT parameters in the RSM table and experimental results are shown in Table 2. Typical machined WEDT component is shown in Fig. 2. ANOVA and response surfaces are used to determine the effect of input WEDT parameters, which are obtained from Design-Expert software. The response MRR is calculated using the following formula:

$$\text{MRR} = \frac{\text{Total volume removed from the workpiece}}{\text{Time taken}} \text{ mm}^3/\text{min}. \quad (1)$$

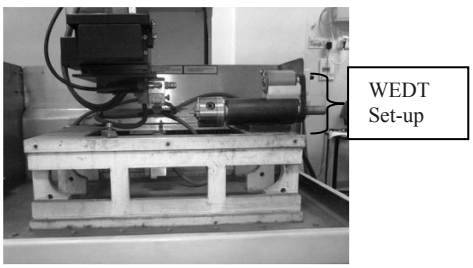

Fig. 1. Photograph of the WEDT setup installed in the WEDM

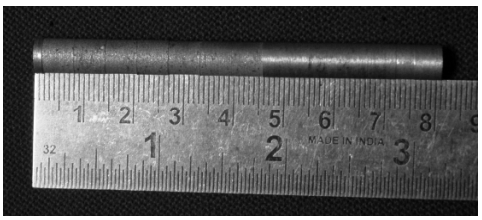

Fig. 2. Photograph of the typical WEDT workpiece

Table 1. Input process parameters and their levels

Parameter	Low	Centre	High
Pulse on time [T_{ON}] (µs)	6	8	10
Gap voltage [V] (Volts)	45	50	55
Spindle speed [SS] (rpm)	125	150	175

3. Results and discussion

Table 3 shows ANOVA results obtained for the MRR. It indicates that among the input process parameters studied in this work, the individual effect of T_{ON} is found to be significant, while V and SS are found to be insignificant. However, the quadratic effect of the V is also found to be significant (Table 3). The relationship between the input parameters and the response MRR is expressed in the form of regression equation and it is given below:

$$\text{MRR} = -175.29 + 7.24*T_{ON} + 6.45*V - 0.144*SS - 0.043*T_{ON}*V - 0.014*T_{ON}*SS - 0.006*V*SS - 0.14*T_{ON}^2 - 0.051*V^2 + 0.002*SS^2 \quad (2)$$

Table 2 WEDT parameters and experimental results

Ex. No	T_{ON} (µs)	V (Volts)	SS (rpm)	MRR (mm^3/min)
1	6	45	150	6.99
2	10	45	150	10.17
3	6	55	150	8.38
4	10	55	150	9.84
5	6	50	125	8.97
6	10	50	125	14.26
7	6	50	175	9.71
8	10	50	175	12.15
9	8	45	125	8.28
10	8	55	125	11.56
11	8	45	175	10.93
12	8	55	175	11.36
13	8	50	150	10.81
14	8	50	150	10.76
15	8	50	150	10.45

Table 3 ANOVA table of MRR

S	SS	Dof	M	F	P
*Model	39.80	9	4.42	5.57	0.036
*T_{ON}	19.13	1	19.13	24.08	0.004
V	2.84	1	2.84	3.58	0.117
SS	0.15	1	0.15	0.18	0.686
T_{ON} x V	0.74	1	0.74	0.93	0.378
T_{ON} x SS	2.03	1	2.03	2.56	0.170
V x SS	2.03	1	2.03	2.56	0.170
T_{ON}^2	1.09	1	1.09	1.38	0.293
*V^2	6.09	1	6.09	7.67	0.039
SS^2	4.83	1	4.83	6.08	0.056
Residual	3.97	5	0.79	-	-
Lack of Fit	3.90	3	1.30	34.14	0.028
Pure Error	0.08	2	0.04	-	-
Cor Total	43.77	14	-	-	-

*Significant, S- Source, SS-Sum of square, Dof- Degree of freedom, M- Mean Square, F- F value, P- P value.

Fig. 3 indicates response surface of MRR by varying the SS and V, while T_{ON} is held constant at low level [Fig. 3

(a)], medium level [Fig. 3 (b)] and high level [Fig. 3 (c)]. Fig. 3a indicates that with low T_{ON}, higher MRR is achievable with low SS and V in between medium and high level (50 V to 55 V). The maximum MRR achievable with this combination is found to be 10.3 mm^3/min. Fig. 3 (b) indicates that with medium T_{ON}, higher MRR is achievable with V in between medium and high level (50 V to 55 V) and low SS. The maximum MRR is found to be 11.9 mm^3/min. Fig. 3c indicates that with high T_{ON}, higher MRR is achievable with V in between medium and high level (50 V to 55 V) and low SS. The maximum MRR is found to be 13.4 mm^3/ min. By comparing the influence of different levels (low, medium and high) of T_{ON} from Fig. 3, it is observed that high T_{ON} results in higher MRR. High T_{ON} generates high discharge energy and therefore creates wide and deep craters in the workpiece surface, which leads to higher MRR [2,4,12,13].

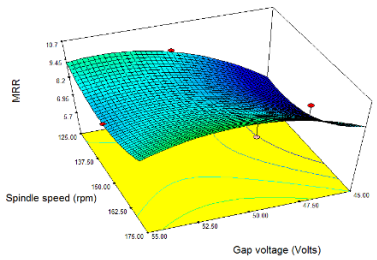

a) Spindle speed Vs Gap voltage (at low T_{ON})

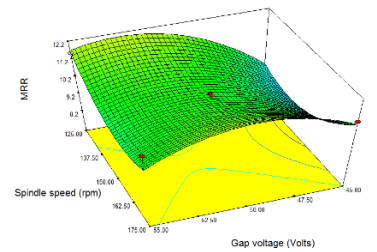

b) Spindle speed Vs Gap voltage (at medium T_{ON})

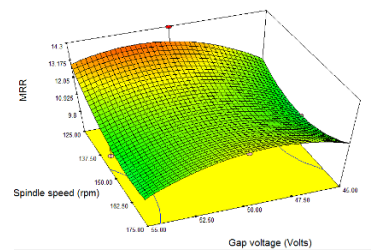

c) Spindle speed Vs Gap voltage (at high T_{ON})

Fig. 3 Response surface of MRR at various T_{ON} levels

Fig. 4 indicates response surface of MRR by varying the SS and T_{ON}, while V is maintained at low level [Fig. 4 (a)], medium level [Fig. 4 (b)] and high level [Fig. 4 (c)]. Figure 4 (a) indicates that with low V, higher MRR is achievable with T_{ON} at its high level and low SS. The maximum MRR is found to be around 11.4 mm^3/ min. Fig. 4 (b) indicates that with medium V, higher MRR is achievable with low SS and high T_{ON}. The maximum MRR is found to be around 13.4 mm^3/ min. Fig 4 (c) indicates that with high V, higher MRR is achievable with low SS and high T_{ON}. The maximum MRR is found to be around 13 mm^3/min. By comparing the influence of different levels (i.e. low, medium and high) of V from Fig. 4, it is observed that medium V results in higher MRR. The high V also results in nearly similar value. However, the use of high V is not advisable because it will increase the manufacturing cost (high wear rate of the wire), lead to arcing and also increase the rate of deposition of resolidification/recast layer on the workpiece [12,13]. Hence, medium V is preferable for higher productivity and continuous machining without breakage of wire electrode.

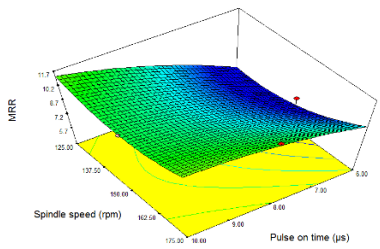

a) Spindle speed Vs Pulse on time (at low V)

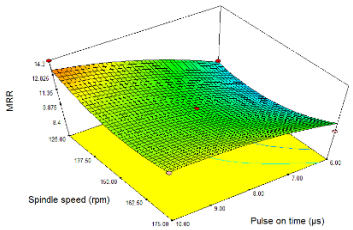

b) Spindle speed Vs Pulse on time (at medium V)

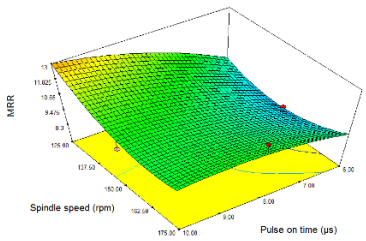

c) Spindle speed Vs Pulse on time (at high V)

Fig. 4 Response surface of MRR at various V levels

Fig. 5 indicates response surface of MRR by varying the T_{ON} and V, while SS is held constant at low level [Fig. 5

(a)], medium level [Fig. 5 (b)] and high level [Fig. 5 (c)]. Fig. 5 (a) indicates that with low SS, higher MRR is achievable by maintaining the V between medium level to high level and the T_{ON} at its high level. The maximum MRR is found to be around 13.1 mm^3/min. Fig. 5 (b) indicates that with medium SS, higher MRR is achievable with high T_{ON} and V between medium and high level. The MRR achievable with this combination is found to be around 11.7 mm^3/min. Fig. 5 (c) indicates that at with high SS, higher MRR is achievable between medium and high V and T_{ON} at its high level. The maximum MRR is found to be 12.2 mm^3/min. By comparing the influence of different SS levels from Fig. 5, it is observed that low SS results in higher MRR. Low SS may increase the temperature concentration on the workpiece surface during machining compared to that of medium and high SS and hence results in the increased MRR. Low SS may also effectively improve the circulation of the dielectric fluid in the spark gap and enhances the MRR [2,4].

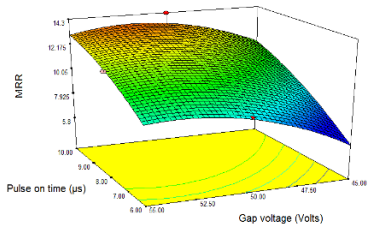

a) Pulse on time Vs gap voltage (at low SS)

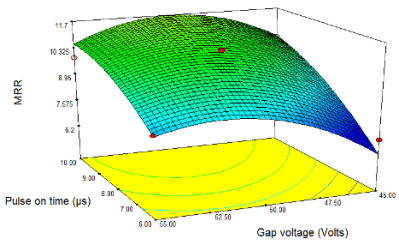

b) Pulse on time Vs gap voltage (at medium SS)

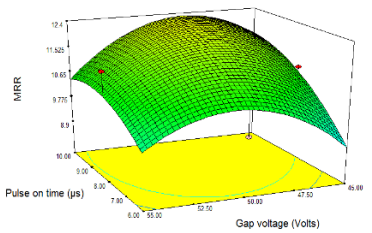

c) Pulse on time Vs gap voltage (at high SS)

Fig. 5 Response surface of MRR at various SS levels

4. Conclusion

The influence of WEDT process parameters such as T_{ON}, V and SS on MRR are analysed for machining of Al/SiC_p MMC. The experiments are carried out as per RSM using Box-Behnken method. The significant parameters and their levels are identified for achieving higher MRR with the help of ANOVA and response surfaces. It is found that high T_{ON}, medium V and low SS leads to higher MRR and effective machining. Hence, these combinatons are recommended for WEDT of Al/SiC_p MMC in order to achieve higher MRR. Regression equation is established for MRR for easier predication.

References

[1] Haddad MJ, Alihoseini F, Hadi M, Hadad M, Tehrani AF, Mohammadi A, (2010) An experimental investigation of cylindrical wire electrical discharge turning process. Int J Adv Manuf Tech 46:1119-1132

[2] Qu J, Shih AJ, Scattergood RO, (2002) Development of the cylindrical wire electrical discharge machining process Part 1: Concept, design, and material removal rate. J Manuf Sci and Engg 124:702-707

[3] Qu J, Shih AJ, Scattergood RO, (2002) Development of the cylindrical wire electrical discharge machining process Part 2: Surface integrity and roundness. J Manuf Sci and Engg 124: 708-714

[4] Mohammadi A, Tehrani AF, Emanian E, Karimi D, (2008) Statistical analysis of wire electrical discharge turning on material removal rate. J Mat Proc Tech 205:283-289

[5] Mohammadi A, Tehrani AF, Emanian E, Karimi D, (2008) A new approach to surface roughness and roundness improvement in wire electrical discharge turning based on statistical analyses. Int J Adv Manuf Tech 39:64-73

[6] Haddad MJ, Tehrani AF, (2008) Material removal rate (MRR) study in the cylindrical wire electrical discharge turning (CWEDT) process. J Mat Proc Tech 199:369-378

[7] Haddad MJ, Tehrani AF, (2008) Investigation of cylindrical wire electrical discharge turning (CWEDT) of AISI D3 tool steel based statistical analysis, J Mat Proc Tech 198:77-85

[8] Matoorian P, Sulaiman S, Ahmad MMHM, (2008) An experimental study of optimization of electrical discharge turning (EDT) process. J Mat Proc Tech 204:350-356

[9] Janardhan V, Samuel GL (2010) Pulse train data analysis to investigate the effect of machining parameters on the performance of wire electro discharge turning (WEDT) process. Int J Mach Tools Manuf 50:775-788

[10] Chawla N, Chawla KK (2006) Metal matrix composites, Springer, Newyork, USA

[11] Montgomery DC (2001) Design and analysis of experiments. John Wiley & Sons, Singapore

[12] Satishkumar D, Kanthababu M, Vajjiravelu V, Anburaj R, Thirumalai Sundarrajan N, Arul H (2011) Investigation on wire electrical discharge machining characteristics of Al6063/SiCp composites. Int J Adv Manuf Tech 56: 975-986

[13] Garg RK, Singh KK, Sachdeva A, Sharma VS, Ojha K, Singh S (2010) Review of research work in sinking EDM and WEDM on metal matrix composite materials. Int J Adv Manuf Tech 50:611-624.

Study on electrolyte jet machining of cemented carbide

K. Mizugai[1], N. Shibuya[2] and M. Kunieda[1]
[1] Department of Precision Engineering, The University of Tokyo, Tokyo, Japan
[2] Department of Mechanical Systems Engineering, Tokyo University of Agriculture and Technology, Tokyo, Japan

Abstract. In this study, electrolyte jet machining (EJM) was attempted on cemented carbide. $NaNO_3$ aqueous solution was used as the electrolyte instead of NaOH aqueous solution, which is normally used for the electrochemical machining of cemented carbide, because of its hazardous characteristics. The machining was carried out with alternating current (AC) because it enables more localized dissolution under the jet than direct current (DC), however an insulator nozzle was additionally employed during AC machining, and was found to be effective for preventing nozzle wear often seen in AC machining as well as for obtaining more localized dissolution area even in DC machining.

Keywords: Electrolyte jet machining, ECM, micro machining, cemented carbide, insulator nozzle

1. Introduction

In electrolyte jet machining (EJM) [1, 2], the workpiece is machined only in the area which is hit by the electrolyte jet by applying an electrical current through the jet. By translating the jet on the workpiece, intricate patterns can be fabricated without the use of special masks [3], since the distribution of current density is localized under the jet [4]. Given that electrolyte jet machining is an electrochemical process, no burrs, cracks, or heat affected zones are generated on the machined surface. Kunieda et al. [3] has therefore been using this method for texturing micro indents on the surface of rolling bearings to extend fatigue life. Moreover, because most electrically conductive materials can be machined regardless of their hardness, this method can be applied to the machining of cemented carbide. However, use of pure $NaNO_3$ or NaCl aqueous solution results in the formation of a tungsten oxide layer on the workpiece surface which hinders the further dissolution of tungsten carbide (WC). Although WC grains can be dissolved by an electrolyte containing NaOH [5], this hazardous electrolyte cannot be used in EJM, because electrolyte mist is generated when the electrolyte is hitting the workpiece surface. On the other hand, Masuzawa et al. [6] succeeded in the electrochemical surface finishing of cemented carbide using harmless $NaNO_3$ solution as the electrolyte with bipolar pulse current, based on the fact that NaOH is generated on the cathode surface during the process. For this reason, the authors attempted the machining of cemented carbide by EJM using $NaNO_3$ aqueous solution in this study. To obtain higher machining accuracy, choice of jet nozzle materials and machining current conditions were also investigated.

2. Electrolyte jet machining (EJM)

2.1. Principle of EJM

Electrolyte jet machining is carried out by jetting electrolytic aqueous solution from a nozzle towards the workpiece while applying voltage between the nozzle and workpiece. When the electrolyte jet hits a plate at a sufficiently high velocity, it flows radially outwards in a fast thin layer which suddenly increases in thickness. Equipotential surfaces in the jet at this time are shown in Fig. 1 (a) and distribution of the current density is concentrated in the area under the jet as shown in Fig.

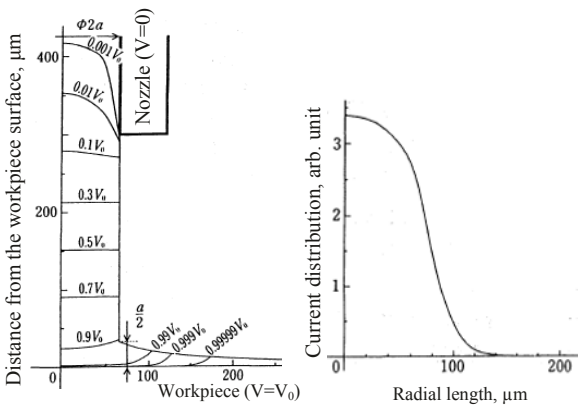

Fig. 1. Analysis of potential and current distribution in EJM [4]

1(b) [4]. Thus, electrolytic dissolution is limited to the jet impinging area. The following is the chemical reaction on the anode surface in the electrochemical machining of cemented carbide using a mixed solution of NaOH and NaCl as the electrolyte [5]. Co is oxidized into Co^{2+}.

$$Co \rightarrow Co^{2}+2e^{-} \quad (1)$$

WC is oxidized into WO_3, thereby forming a thin oxide film on the anode surface. Then NaOH reacts with WO_3 as:

$$WO_3+2NaOH \rightarrow Na_2WO_4+H_2O \quad (2)$$

Since the oxide layer of WO_3 is removed, machining can progress. If NaOH is not mixed into the $NaNO_3$ solution, WO_3 film cannot be removed, thus machining is prevented. On the other hand, the following reaction occurs on the cathode surface in parallel to the reaction of hydrogen gas generation.

$$2H_2O+2Na+2e^{-} \rightarrow 2NaOH+H_2\uparrow \quad (3)$$

In EJM using direct current (DC), since NaOH formed on the inner surface of the cathode nozzle is transferred to the surface of the anode workpiece by the convection of the jet, NaOH need not to be added to the electrolyte prior to machining. Using alternating current (AC), as Masuzawa et al. [6] found in the electrochemical surface finishing of cemented carbide with $NaNO_3$ aqueous solution, the WO_3 film formed on the workpiece surface when the workpiece serves as the anode can be removed by NaOH which is generated when the workpiece serves as cathode. Hence in EJM, cemented carbide can be machined using either DC or AC current.

2.2. Experimental equipment

Figure 2 shows the experimental setup. The workpiece was fixed in a work tank whose position was controlled horizontally using an XY table. The nozzle was installed on the Z table to adjust the gap width between the nozzle and workpiece. The electrolyte was supplied from the pressure tank pressurized by an air compressor.

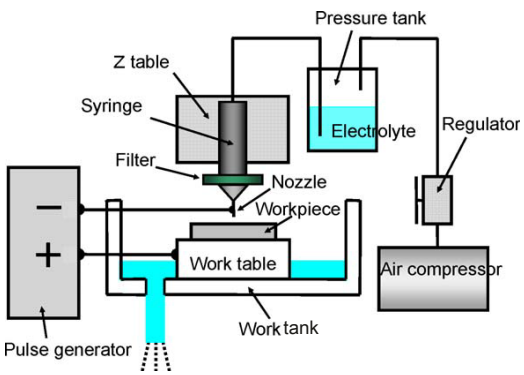

Fig. 2. Experimental equipment

3. Pit machining of cemented carbide

3.1. DC machining

NaOH generated on the inner surface of the cathode nozzle is transferred to the workpiece surface in EJM. Based on this idea, pits were machined on a cemented carbide plate using a standing jet of $NaNO_3$ aqueous solution, through which DC current was supplied. The machining conditions are shown in Table 1. A metallic cylindrical nozzle ϕ400μm in inner diameter was used. The cross-sectional view of a machined pit is shown in Fig. 3(a). The diameter of the machined area was over four times larger than the nozzle inner diameter. This is because the NaOH concentration distributed widely. From the equipotential surfaces in the jet shown in Fig. 1(a) calculated by Yoneda et al. [4], it is found that NaOH is mostly generated at the inner edge of the nozzle outlet where the potential gradient is steep. Hence, the NaOH concentration is highest on the side surface of the cylindrical jet but lowest at the center. As shown in Fig. 4, since NaOH is transferred to the workpiece surface

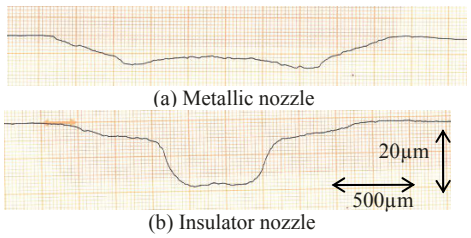

(a) Metallic nozzle

(b) Insulator nozzle

Fig. 3. Cross-sectional view of pits machined using

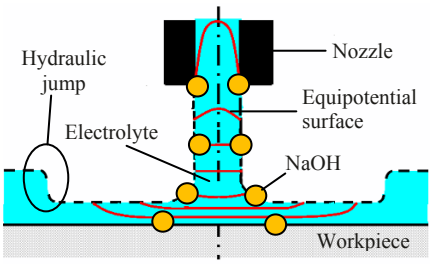

Fig. 4 Flow of NaOH

Table 1. Machining conditions in pit machining

Nozzle inner diameter [μm]	ϕ 400
Gap width between nozzle and workpiece [mm]	4.0
Tank pressure [MPa]	0.5
Machining current [mA]	30
Machining time [s]	30
Work material	Cemented carbide V30 (WC particle size : 1.0-2.5μm)

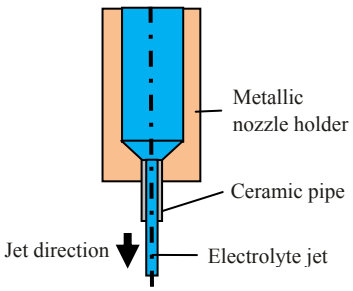

Fig. 5 Insulator nozzle

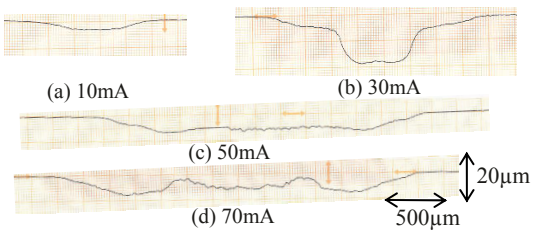

Fig. 6 Influence of current on pit shape with DC current

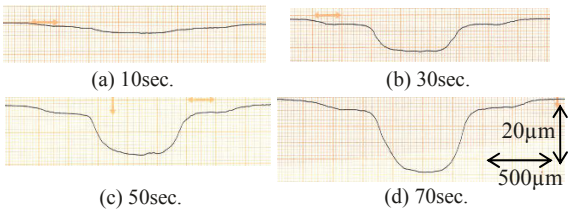

Fig. 7. Influence of machining time on pit shape with DC current

without mixing into the center of the jet, machining mostly occurs in the periphery of the jet colliding area. This finding led to the idea of using the insulator nozzle shown in Fig. 5. Since NaOH is generated in the hollow space of the metallic nozzle holder, NaOH concentration tends to become uniform due to the turbulent flow before the electrolyte flows into the ceramic pipe. Figure 3 (b) shows the cross-section of a pit machined using the insulator nozzle under the same conditions as those shown in Table 1. It was found that the insulator nozzle is effective for realizing selective machining under the jet. Figures 6 and 7 show the effects of machining current and time on the pit shape, respectively. The other conditions used were the same as those in Table 1. Fig. 6 shows that excessive currents larger than 30mA cause enlargement of the machined pit area with decreased pit depth. Fig. 7 shows that the pit becomes deeper proportionally to the machining time under the conditions used in the experiment.

3.2. AC machining

Even if NaOH is not mixed in the $NaNO_3$ aqueous solution, NaOH can be generated on the workpiece surface while the polarity of the workpiece is negative using AC current. Masuzawa et al. [6] employed this reaction and succeeded in the electrochemical surface finishing of cemented carbide using AC current. With AC current, the NaOH generated when the workpiece polarity is negative dissolves the WO_3 film formed over the workpiece when the workpiece polarity is positive. Hence, cemented carbide can be machined by EJM using AC current. To prove this idea, we machined pits on cemented carbide using the same cylindrical metallic nozzle as that described in Section 1.3.1 with an AC rectangular pulse current of ±30mA at a frequency of 5Hz. Fig. 8 (a) shows the cross-section of the pit machined. The comparison between Fig. 8 (a) and Fig. 3 indicates that the diameter of the pit machined with AC current is smaller than that with DC current. With the metallic nozzle however, the inner edge of the nozzle outlet wears out when the polarity of the nozzle is positive, resulting in deformation of the jet. Fig. 9 shows the cross-sections of a metallic nozzle at the outlet before and after the machining time of 15 min. The inner edge of the nozzle outlet wore preferentially because the current density was highest at the edge as indicated by Fig. 1(a). To solve this problem, the insulator nozzle in Fig. 5 was applied to the AC machining. As shown in Fig. 8 (b), the diameter of the pit machined using the insulator nozzle was twice as large as the nozzle inner diameter, a little larger than the case of the metallic nozzle shown in Fig. 8 (a). This is probably because the jet shape was not parallel in the case of the ceramic nozzle because it was not built specifically for this study. We investigated the effects of peak current, machining time, and current frequency on the shape of the pits machined using the insulator nozzle, as shown in Figs. 10, 11, and 12, respectively. Machining conditions other than these were

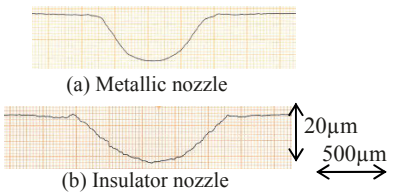

Fig. 8 Cross-section of pit machined with AC (5Hz)

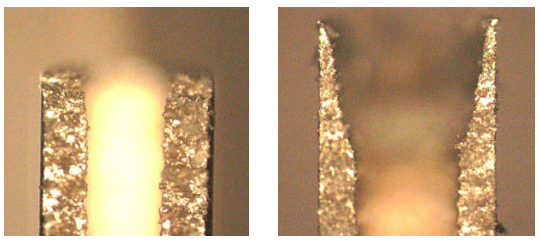

Fig. 9. Wear of metallic nozzle at outlet in AC machining

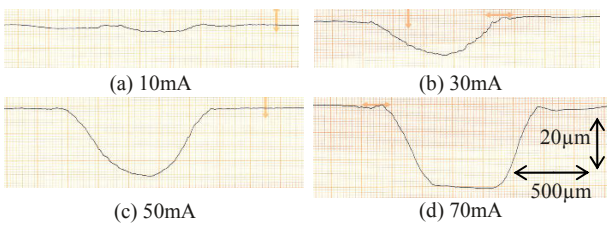

Fig. 10. Influence of peak current on pit shape with AC current

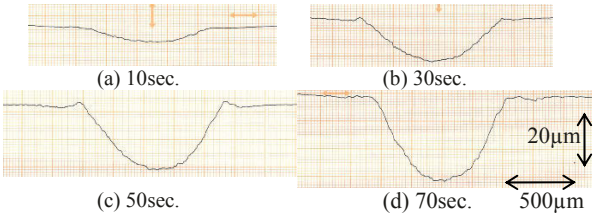

Fig. 11 Influence of machining time on pit shape with AC current

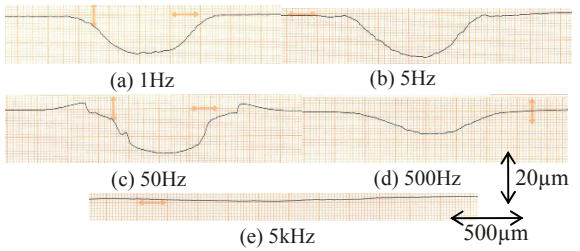

Fig. 12. Influence of current frequency on pit shape with AC current

the same as those used in Fig. 8. Although higher machining current resulted in deeper pit depth, excessive current led to saturation in the pit depth. The machined depth increased proportionally to the machining time. Figure 12 shows that the optimal frequency of the AC current was 5 Hz.

4. Observation of machined surface

Figure 13 shows the SEM images of the micro structures on the bottom surface of the pits machined by EJM under the machining conditions in Table 1. It can be seen from Figure 13 (c) that WC grains were removed more preferentially than Co binder with AC current of 5Hz, where machining rate was comparatively high. On the other hand, Figs. 13 (b) and 13 (d) show that the Co binder was dissolved selectively leaving WC grains on the surface in machining using DC current and AC current with 50 Hz, where machining rate was low.

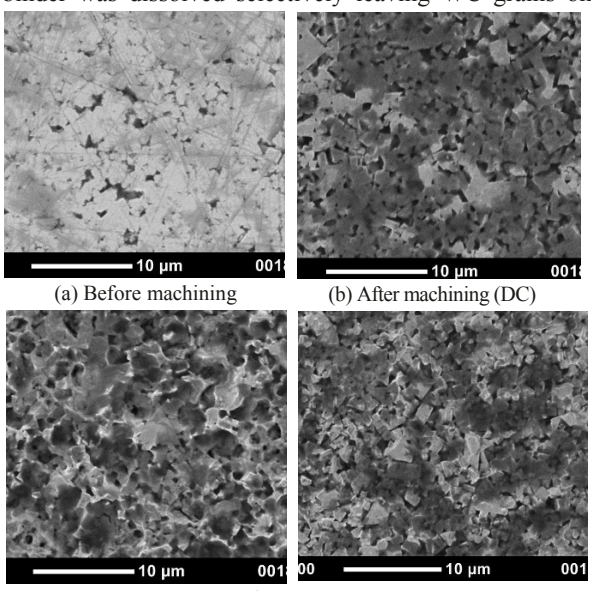

(a) Before machining (b) After machining (DC)
(c) After machining (5Hz) (d) After machining (50Hz)

Fig. 13 Micro structure of surface machined by EJM

5. Conclusions

In the EJM of cemented carbide with DC current, NaOH generated in the cathode nozzle is transferred by the jet to the workpiece surface, where WO_3 film is removed, thereby allowing material removal to progress. The newly developed insulator nozzle enables more localized dissolution under the jet impinging area than metallic nozzle. Although AC current realizes more localized machining than DC current, the inner edge of the metallic nozzle wears out. Thus, the insulator nozzle is useful for preventing nozzle wear when machining with AC current.

Acknowledgements: This work was supported by the Grant-in-Aid for Challenging Exploratory Research from the Japan Society for the Promotion of Science (23656096).

References

[1] Ippolito R, Tornincasa S, Capello G (1981) Electron-Jet Drilling. Annals of the CIRP 30(1):87–89.
[2] Kozak J (1989) Some Aspects of Electro Jet Drilling. 4th International Conference on Developments in Production Engineering Design & Control, 363.369.
[3] Kunieda M, Yoshida M, Yoshida H, Akamatsu Y (1993), Influence of Micro Indents Formed by Electro-chemical Jet Machining on Rolling Bearing Fatigue Life, ASME, PED-Vol64, 693-699.
[4] Yoneda K, Kunieda M (1996) Numerical Analysis of Cross Section Shape of Micro-Indents Formed by the Electrochemical Jet Machining. Journal of JSEME 29(63):1-8. (in Japanese)
[5] Maeda S, Saito N, Haishi Y (1967), Principle and Characteristics of Electro-Chemical Machining. Mitsubishi Denki Giho, 41(10): 1267-1279 (in Japanese)
[6] Masuzawa T, Kimura M (1991), Electrochemical Surface Finishing of Tungsten Carbide Alloy, Annals of the CIRP, 40(1):199-202.

The material removal rate increases during machining of the steel St 37 (DIN 17100) in the electrical discharge machining process

S. Santos, A. Gomes and J. D. Marafona
Departamento de Engenharia Mecânica, Faculdade de Engenharia da Universidade do Porto
Rua Dr. Roberto Frias, 4200-465 Porto, Portugal

Abstract. In this article is shown that the material removal rate increases with machining time, until a peak in the material removal rate be reached for a depth of cut, followed by its decrease with the increase of the depth of cut. This statement is opposite to that says that material removal rate decreases with machining time followed by a stabilization. The increase of the material removal rate depends more on the pulse duration, than of the current intensity. There is a fast increase in the material removal rate until the peak be reached when small pulses are used, in opposition to a slow increase when long pulses are used. The material removal rate is low for small machining times independently of the pulse duration and current intensity. This behavior of the material removal rate was found for the current intensities and duration of pulses used. Thus, the research shows not only that the material removal rate increases during machining time, in opposition to the idea that it decreases, but also that the material removal rate decreases for a depth of machining due to the degradation of the machining conditions. Therefore, the increase of the material removal rate is due to the machining conditions (debris particles in the gap) and/or occurrence a metallurgical modification.

Keywords: Electrical discharge machining (EDM); machining depth; debris particles; gap flushing; Material removal rate (MRR).

1. Introduction

Electrical discharge machining (EDM) is a non-traditional manufacturing process where the material is removed by a succession of electrical discharges, which occur between the electrode and workpiece that are submersed in a dielectric fluid, such as, kerosene or deionised water. The electrical discharge machining process is widely used in the machining of hard metals and its alloys in the aerospace, automobile and moulds industries.

The flushing of debris particles and the cooling of dielectric fluid in the gap are critical characteristics to prevent the same localization and concentration of discharges [1]. The debris particles play a role in the ocurrence of the discharge in the electrical discharge machining (EDM) [2]. So, the stability of electrical discharges for small depths of cut is easily achieved by replacement of the contaminated dielectric fluid with a fresh one.

The material removal rate increases due to the interactions of workpiece hardness and EDM input parameters [3]. The workpiece hardness is obtained with heat treatments, so, being the electrical discharge machining characterized by a electric-thermal phenomenon, leads to the ocurrence of metalurgical modification of the base material of the workpiece [4].

On the one hand, it is known that the material removal rate decreases when there is a decrease in the surface roughness of the workpiece. On the other hand, the material removal rate increases simultaneously with the reduction of surface roughness of workpiece, according to Abbas et al. [5]. Only, the metallurgical modifications of the base material of the workpiece explains the latter statement. Therefore, the authors decided to investigate the effect of cut depth on material removal rate and electrode wear rate in a low carbon steel – St 37 (DIN 17100) using the flushing of debris with dielectric fluid at a pressure of 1bar.

2. Experimental methodology

This methodology was designed and performed in a die-sinking EDM machine, AGIE COMPACT 3, equipped with adaptive control facilities. The adaptive control optimization (ACO) system enables the process to be optimized automatically and it was switched off so that the results can be generalized to all machines. The electrode and workpiece materials are electrolytic copper and steel DIN 17100-St 37, respectively. The workpiece was a parallelepiped with dimensions of 300x60x25 mm3. The electrodes used were copper rods 16 mm in diameter and a length of 100 mm. The EDM performance is related to the efficiency, which is determined in the EDM process by the material removal rate and tool wear rate. Quality is determined by the accuracy and surface roughness.

Three values of current intensity together with three pulse duration values were used in the experiments and the remaining input parameters were taken from the handbook of the AGIE manufacturer. So, the experiments were realized with the current intensities of 19.3A, 25.4A and 37.1A, together with duration pulses of 18μs, 75μs and 420μs.

This experimental methodology enables determine the cut depth as a significant contributor to the material removal rate for different cut depths with flushing of debris with dielectric fluid at a pressure of 1bar.

3. Experimental results

The experimental results obtained in the research, using the die-sinking EDM machine AGIE COMPACT 3, were analyzed to check the removing of material during the cut depth. On one hand, it is well accepted that material removal decreases with machining time due to the large number of debris in the gap, causing instability in the machining. On the other hand, some authors point out that the cleaning conditions of the dielectric in the beginning of the machining are not favorable to a good machining.

The authors of the research intend to demonstrate that the material removal rate in the beginning of the machining is smaller than during machining.

3.1. Effect of machining depth on material removal rate

Large cut depths are a factor of instability, because the debris particles that are in the gap are difficult to flush with fresh dielectric under pressure. However, the flushing of debris particles can be done without difficulties for small depths of cut and so, it would be expected to increase in the material removal rate for small depths of cut. Marafona and Araújo [3] pointed out that the workpiece hardness and its interactions with input parameters affect the EDM performance. So, the authors studied these effects on steel with low content of carbon St 37 (DIN 17100). Therefore, the material removal rate was evaluated for the cut depths of 1mm, 6mm and 12mm.

The effect of cut depth on material removal rate for the current intensity of 19.3A is analyzed in Fig.1. From the Figure is demonstrated that the material removal rate is smaller for the cut depth of 1mm, independently of the pulse duration used. The maximum removal rate seems to be achieved between the depth of 6mm and 12mm, follow by a degradation of the machining conditions. Figure 2 and 3 show that the material removal rate found in similar conditions of machining for the current intensities of 25.4A and 37.1A. The results are very similar to the current intensity of 19.3A presented in Fig. 1.

The current intensities of 19.3A, 25.4A and 37.1A show a maximum rate of removal material of 45.0mm3/min, 54.1mm3/min and 83.2mm3/min respectively. These maximum values were obtained using the pulse duration of 420μs and the cut depth of 12mm. So, one can conclude that the material removal rate increases with the increase of the cut depth and after there is a degradation of the machining conditions that leads to a decrease in the material removal rate.

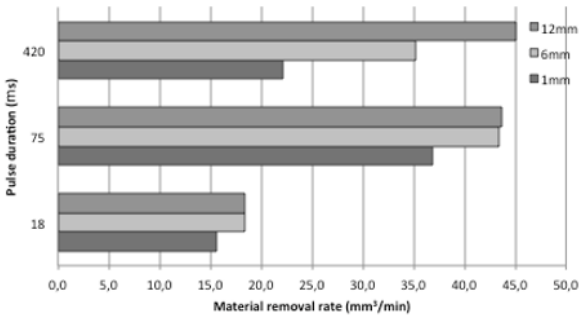

Fig. 1 Effect of machining depth on MRR for the current intensity of 19.3A.

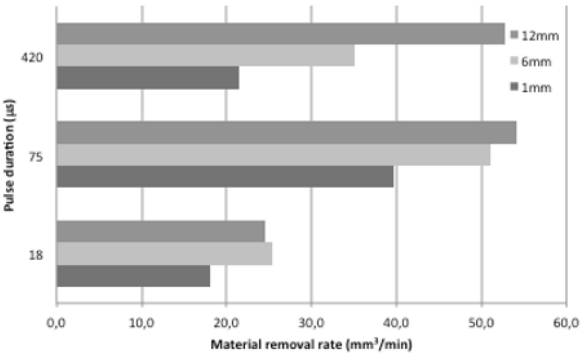

Fig. 2 Effect of machining depth on MRR for the current intensity of 25.4A.

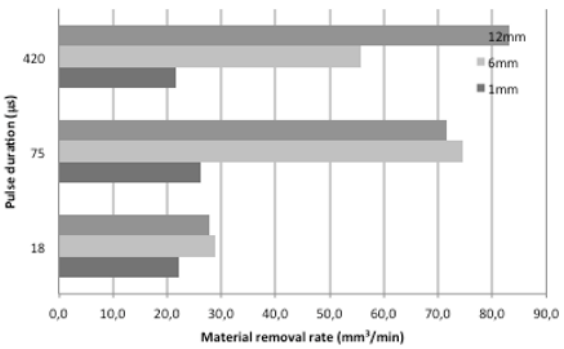

Fig. 3 Effect of machining depth on MRR for the current intensity of 37.1A.

In Fig. 1 is shown that the material removal rate is higher for the pulse duration of 75μs and the cut depths of 1mm and 6mm. This behaviour is followed by other current

intensities as shown in Fig. 2 and 3, being this behaviour according to the trend of the material removal rate with the pulse duration.

Therefore, the research demonstrates that the material removal rate increases with the increase of cut depth,which is opposite to the idea that the material removal rate decreases and tends to a constant value during the machining.

4. Conclusion

The research results show that the material removal rate is affected by machining cut depth. This is demonstrated by the experimental results using the steel, St 37 (DIN 17100) that has a very small amount of carbon, and so, passible to have great changes in its metallurgical structure. As, main conclusion the authors can to say that there is an increase in the material removal rate with the increase of machining cut depth, followed by a degradation of the machining conditions, which lead to a decrease in the material removal rate, when is used the steel St 37 (DIN 17100).

References

[1] Kunieda M., Lauwers B., Rajurkar K.P.,Schumacker B.M., (2005) Advancing EDM through Fundamental Insight into the Process, Annals of the CIRP, 54 (2) 599-622.

[2] Schumacker B.M., (1990) About the Role of Debris in the Gap During Electrical Discharge Machining, Annals of the CIRP, 39 (1) 197-199.

[3] Marafona J.D., Araújo A., (2009) Influence of workpiece hardness on EDM performance, International Journal of Machine Tools & Manufacture, 49 (9) 744-748.

[4] Soni J.S., Chakraverti G., (1996) Experimental investigation on migration of material during EDM of Die steel (T215Cr12), Journal of Material Processing Technology, 56 439-451.

[5] Abbas N.M., Solomon D.G., Bahari Md. F., (2007) A review on current research trends in electrical discharge machining, International Journal of Machine Tools & Manufacture, 47 1214-1228.